ResearchGate

See discussions, stats, and author profiles for this publication at: https://www.researchgate.net/publication/221947914

Eu(III) adsorption/desorption on Na-bentonite: Experimental and modeling studies

ARTICLE *in* COLLOIDS AND SURFACES A PHYSICOCHEMICAL AND ENGINEERING ASPECTS · MAY 2009

Impact Factor: 2.75 · DOI: 10.1016/j.colsurfa.2009.02.007

CITATIONS
42

READS
85

6 AUTHORS, INCLUDING:

Zhijun Guo
Lanzhou University
45 PUBLICATIONS **419** CITATIONS
SEE PROFILE

Keliang Shi
Lanzhou University
18 PUBLICATIONS **196** CITATIONS
SEE PROFILE

Wangsuo Wu
Lanzhou University
121 PUBLICATIONS **1,690** CITATIONS
SEE PROFILE

All in-text references underlined in blue are linked to publications on ResearchGate, letting you access and read them immediately.

Available from: Keliang Shi
Retrieved on: 02 February 2016

Colloids and Surfaces A: Physicochem. Eng. Aspects 339 (2009) 126–133

Contents lists available at ScienceDirect

Colloids and Surfaces A: Physicochemical and Engineering Aspects

journal homepage: www.elsevier.com/locate/colsurfa

Eu(III) adsorption/desorption on Na-bentonite: Experimental and modeling studies

Zhijun Guo*, Jiang Xu, Keliang Shi, Yuqin Tang, Wangsuo Wu, Zuyi Tao

Radiochemistry Lab, School of Nuclear Science and Technology, Lanzhou University, 730000, Lanzhou, China

ARTICLE INFO

Article history:
Received 28 December 2008
Received in revised form 1 February 2009
Accepted 6 February 2009
Available online 14 February 2009

Keywords:
Potentiometric titration
Na-bentonite
Eu(III)
Adsorption
Desorption
Surface complexation
Modeling

ABSTRACT

In this paper, the physico-chemical, titration and Eu(III) adsorption/desorption characteristics of a purified Na-bentonite have been measured. Potentiometric titration at three ionic strengths (0.01, 0.1 and 0.5 mol/L NaCl) at 25 °C indicates that the point of zero charge (PZC) of the Na-bentonite increases with decreasing ionic strength. The parallel titration curves at three ionic strengths were interpreted by considering a layer site and two edge hydroxyl sites in the framework of surface complexation model. The adsorption/desorption of Eu(III) on the Na-bentonite was investigated by a batch experimental method. pH adsorption edges of Eu(III) in the absence and presence of CO_2 at variable Eu(III) concentrations (6.74×10^{-8} and 3.33×10^{-6} mol/L) were collected and reasonably interpreted by a surface complexation model. Adsorption and desorption isotherms at pHs 4.04 ± 0.05, 6.01 ± 0.05, 6.53 ± 0.05 and 7.46 ± 0.05 indicate that the adsorption/desorption of Eu(III) on the Na-bentonite is reversible. The adsorption isotherms of Eu(III) were successfully reproduced by the proposed model.

© 2009 Elsevier B.V. All rights reserved.

1. Introduction

Bentonite has been considered to be a backfilling material in geological disposal of nuclear waste in many countries. As a main component of bentonite, montmorillonite is a 2:1 layer type phyllosilicate composed of two tetrahedral sheets sandwiching an octahedral sheet. In compacted state, montmorillonite shows low hydraulic conductivity, "self-healing" behavior, and high cation exchange and adsorption capacity [1]. Thus the adsorption of radionuclides on bentonite and montmorillonite has been extensively studied [2–7]

A lot of studies have been focused on setting up thermodynamic models to quantitatively reproduce adsorption of radionuclides from aqueous solutions. Surface complexation model has been demonstrated to be a powerful tool for this purpose [8]. As an analogue of other trivalent lanthanides and actinides, Eu(III) is usually used in adsorption studies to avoid handling α-ray emitters. Therefore, many studies have been carried out on adsorption of Eu(III) on bentonite/montmorillonite. Different models have been developed for these particular adsorption systems. Since 1997, Bradbury and Baeyens have published a series of papers which systematically describe a model called "2-site protolysis no electrostatics surface complexation and cation exchange (2SPNE/CE)" for the adsorption of a number of cations including Eu(III) on Na/Ca-montmorillonite [9–14]. The main feature of this model is that no electrostatic term is needed for the surface complexation reactions. The model is based on the titration results of the Na-montmorillonite by a batch titration method [9] which indicated that the titration curves were insensitive to ionic strengths. This is a contrast to the results obtained by using a potentiometric titration method [15,16]. Tertre et al. [17] proposed another model in terms of surface complexation as well as cation exchange to interpret Eu(III) adsorption on Na-montmorillonite. The model by Tertre et al. was based on potentiometric titration of Na-montmorillonite at three ionic strengths. It was found that the titration curves were sensitive to ionic strengths and parallel to each other [15].

In this paper, the physico-chemical, titration and Eu(III) adsorption/desorption characteristics of a purified Na-bentonite were studied. Potentiometric titration of the Na-bentonite was performed at 25 °C and three ionic strengths. The adsorption of Eu(III) was investigated as functions of pH, Eu(III) concentration, solid-to-liquid ratio (m/V) and partial pressure of CO_2. The main objectives are (i) to experimentally collect adsorption/desorption data of Eu(III) on the purified Na-bentonite under wide experimental conditions, (ii) to study the reversibility of Eu(III) adsorption/desorption on the purified Na-bentonite, and (iii) to set up a reasonable thermodynamic model capable of describing and reproducing the adsorption of Eu(III) on the Na-bentonite.

* Corresponding author. Tel.: +86 931 8913278; fax: +86 931 8913551.
E-mail address: guozhj@lzu.edu.cn (Z. Guo).

0927-7757/$ – see front matter © 2009 Elsevier B.V. All rights reserved.
doi:10.1016/j.colsurfa.2009.02.007

2. Materials and methods

2.1. Chemicals

Eu(III) stock solution was prepared by dissolving Eu_2O_3 (99.99%) in an HCl solution. $^{152+154}$Eu(III) radiotracer was obtained from China Institute of Atomic Energy. All other chemicals used were of analytical grade. All solutions and suspensions were prepared with deionized water (18 MΩ/cm).

2.2. Clay mineral purification

A raw bentonite was supplied by Jinchuan Bentonite Company (Jinchuan, Gansu Province, China). The fraction with diameters <63 μm was collected and dispersed in 0.1 NaCl solution (20 g/L). The pH of the suspension was adjusted to ~3.5 with HCl and kept for 48 h under shaking to remove carbonates. Then the purified bentonite was transformed into Na-form. The fine fraction (<2 μm) was collected by centrifugation method, then washed with ethanol to remove the background electrolyte and finally dried at 45 °C.

2.3. Clay mineral characterization

2.3.1. XRD data

The X-ray diffraction (XRD) patterns of the purified Na-bentonite are shown in Fig. 1. The main component of the purified Na-bentonite is Na-montmorillonite and the major impurity is quartz. The impurities could not be removed completely by centrifugation method because they are fine as the clay particles themselves [18].

2.3.2. SEM measurement and specific surface area

Scanning electron microscopy (SEM) image of the purified Na-bentonite was collected on a JSM-6701F scanning electron microscope. As shown in Fig. 2, the Na-bentonite is mainly composed of flakes, which is agreement with the microscopic observation of montmorillonite reported. The specific surface area of the purified Na-bentonite, determined from N_2 adsorption/desorption isotherms by B.E.T. method, was found to be 53.6 m^2/g.

2.3.3. Composition of Na-bentonite and cation exchange capacity

Usually, the proportion of impurities in clay minerals could not be derived accurately from XRD data [19,20]. Thus the composition of a clay mineral is usually obtained by a combination of bulk chemical analysis and calculations [19,20]. The result of X-ray fluorescence analysis for the purified Na-bentonite is listed in Table 1. According to Fig. 1, the purified Na-bentonite used in this study was assumed to be a mixture of silica and montmorillonite. The proportions of silica and montmorillonite were calculated from the chemical composition to be 12 wt.% SiO_2 and 88 wt.% montmorillonite. The calculated structural formula of the montmorillonite is $[Si(IV)_8](Al(III)_{3.19}, Fe(III)_{0.29}, Fe(II)_{0.38}, Mg(II)_{0.14})O_{20}(OH)_4$ $(Ca(II)_{0.023}, Na(I)_{0.35}, K(I)_{0.127})$. The cation exchange capacity (CEC) calculated from this formula is 694 meq/kg, which implies that the CEC of the purified Na-bentonite should be 694 × 0.88 = 611 meq/kg. The CEC determined by Ni-en (ethylenediamine) extraction method [21] was found to be 623 ± 12 meq/kg.

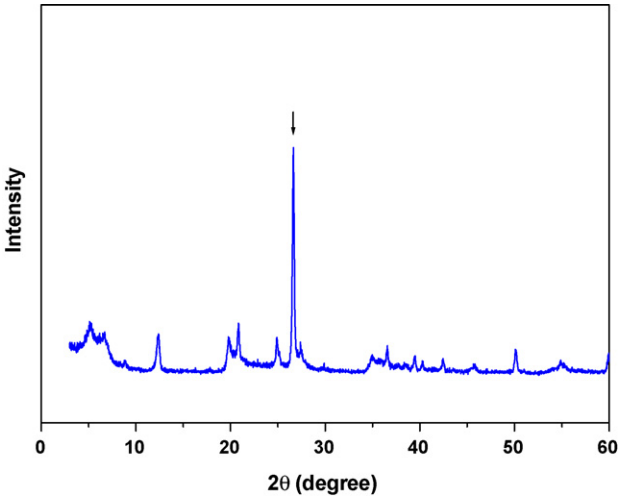

Fig. 1. XRD spectrum of the purified Na-bentonite; the arrow indicates the presence of quartz.

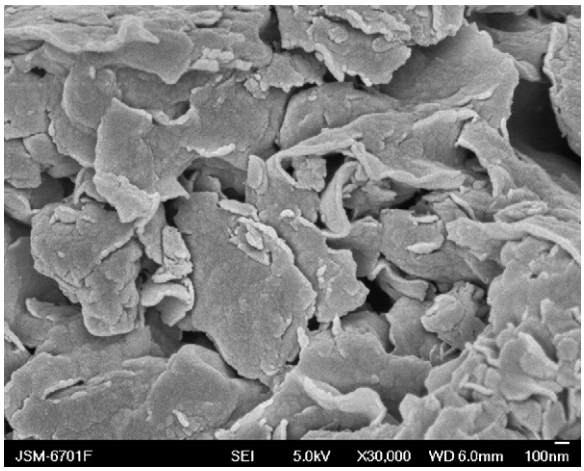

Fig. 2. SEM micrograph of the purified Na-bentonite.

2.4. Potentiometric titration

0.6 g Na-bentonite was dispersed in 60 mL NaCl solution (0.01, 0.1 and 0.5 mol/L). The suspension was stirred under argon atmosphere for 12 h. Then a standard HCl solution (0.05 mol/L) was added to pH ~4. The suspension was titrated with a standard NaOH solution (0.05 mol/L) to pH ~9. Then titration from pH 9 to 4 was carried out sequentially using the standard HCl solution for the same suspension. The incremental volume during titration was fixed at 50 μL. The pH was recorded when the variation of the potential became less than 0.5 mV/min (equivalent to about 0.01 pH units per min.) or the interval was more than 10 min. The total duration of the titration from pH 4 to 9 (or from 9 to 4) was no more than 3 h. Blank titrations were carried out following the same method except that the incremental volume was fixed at 6 μL. The titrations were carried out in a glass vessel on a Metrohm Titrando 709 with a combined electrode (Metrohm 6.026.100). The temperature of the glass vessel was fixed at 25 °C by means of water circulation.

2.5. Adsorption and desorption

All adsorption and desorption experiments were carried out in 0.1 mol/L NaCl solution at 22 ± 2 °C.

Table 1
Chemical composition of the purified Na-bentonite.

Na-bentonite	SiO_2	Al_2O_3	Fe_2O_3	MgO	CaO	Na_2O	K_2O
Wt.%	71.36	19.05	6.22	0.66	0.15	1.27	0.7

2.5.1. Adsorption and desorption in the absence of CO_2

Adsorption and desorption were carried out in a nitrogen atmosphere glove box. The pH of Na-bentonite suspension in polyethylene tube was adjusted with small amounts of HCl and NaOH. For adsorption isotherms at pH 6.5 and 7.5, MES (2-(*N*-morpholino)ethanesulfonic acid) and MOPS (3-(*N*-morpholino)propanesulfonic acid) (2×10^{-3} mol/L) were respectively used as buffers to keep the aqueous pH constant. Desired amount of the Eu(III) stock solution was added and the suspension was spiked with $^{152+154}$Eu(III) radiotracer. The total Eu(III) concentration was obtained from the sum of the stable and radioactive Eu(III) added. Then the suspension was shaken for 5 days. Prior experiments indicated that 5 days is sufficient for the adsorption equilibrium to be reached. Then the pH of the suspension was measured. An aliquot of the suspension was sampled for measuring the radioactivity in the suspension. The solid and aqueous phases were separated by centrifugation at 18,000 × *g* for 30 min. An aliquot of the supernatant was sampled for measuring the radioactivity in aqueous phase.

Desorption isotherm of Eu(III) was collected by a dilution method. When adsorption equilibrium was reached, the suspension was centrifuged and most of the supernatant was exchange with same volume of the background electrolyte solution at same ionic strength and pH. The Na-bentonite was dispersed again and shaken to reach new adsorption equilibrium. Then the suspension was analyzed with the same method above.

2.5.2. Adsorption in the presence of CO_2 ($P_{CO_2} = 10^{-3.58}$ atm)

The pH of the suspension in acidic range was adjusted with HCl. For the suspension at pH > 7, calculated amounts of $NaHCO_3$ and/or Na_2CO_3 were added to obtain a pH around the desired value. Then the suspension was bubbled with air which had been conditioned with 0.1 mol/L NaCl solution for water vapor saturation. When the pH drift of the suspension was less than 0.08 pH units per day, proper amounts of the Eu(III) stock solution and the $^{152+154}$Eu(III) radiotracer were added. The suspensions were shaken and the tubes were opened regularly until adsorption equilibrium to be reached. The methods of analyses were the same as those described above.

2.5.3. K_d calculation

The distribution coefficient of Eu(III) (K_d, L/g) was calculated as:

$$K_d = \frac{q}{C_{eq}} = \frac{(A_0 - A_{eq})}{A_{eq}} \frac{V}{m} \quad (1)$$

where q (mol/g) is the amount of Eu(III) adsorbed, C_{eq} (mol/L) the aqueous Eu(III) concentration, A_0 total radioactivity in the suspension, A_{eq} the radioactivity in the aqueous phase, V (L) the volume of aqueous solution and m (g) the mass of the sorbent.

2.5.4. pH and radioactivity measurements

pH measurements were carried out on a Metrohm 781 pH/ion meter with a combined electrode (Metrohm 6.0234.100). The radioactivity of $^{152+154}$Eu was measured on a Backman LS 6500 liquid scintillation counter.

2.6. Modeling

Double layer model was used to fit the data of the potentiometric titration and those of Eu(III) adsorption on the purified Na-bentonite. The optimization of the modeling parameters for the results of potentiometric titrations was carried out by using the code FITEQL (version 3.1) [22]. The adsorption data of Eu(III) was modeled by the code PHREEQC (version 2.15) [23]. Aqueous activity coefficients were calculated by the Davies equation. Eu(III) aqueous thermodynamic data used in modeling calculations were from Nagra/PSI Chemical Thermodynamic Data Base [24] (see Table 2).

Table 2
Thermodynamic data for aqueous reactions of Eu(III) used in modeling ($I = 0$, $T = 298.15$ K) [24].

Reactions	log$K$
$Eu^{3+} + Cl^- \rightleftharpoons EuCl^{2+}$	1.10
$Eu^{3+} + 2Cl^- \rightleftharpoons EuCl_2^+$	1.50
$Eu^{3+} + H_2O \rightleftharpoons EuOH^{2+} + H^+$	−7.64
$Eu^{3+} + 2H_2O \rightleftharpoons Eu(OH)_2^+ + 2H^+$	−15.1
$Eu^{3+} + 3H_2O \rightleftharpoons Eu(OH)_3^0(aq) + 3H^+$	−23.7
$Eu^{3+} + 4H_2O \rightleftharpoons Eu(OH)_4^- + 4H^+$	−36.2
$Eu^{3+} + CO_3^{2-} \rightleftharpoons EuCO_3^+$	8.1
$Eu^{3+} + 2CO_3^{2-} \rightleftharpoons Eu(CO_3)_2^-$	12.1

3. Results and discussion

3.1. Potentiometric titration

The proton excess of the Na-bentonite (ΔQ^H, mol/g) was determined by subtracting the titration curve of the background electrolyte solution (blank) from that of the Na-bentonite suspension [8].

$$(C_A - C_B)_{susp} = [H^+] - [OH^-] + \Delta Q_{solid} + \Delta Q_{blank} \quad (2)$$

$$(C_A - C_B)_{blank} = [H^+] - [OH^-] + \Delta Q_{blank} \quad (3)$$

$$\Delta Q^H = \frac{V}{m}[(C_A - C_B)_{susp} - (C_A - C_B)_{blank}] \quad (4)$$

where C_A and C_B (mol/L) are the concentrations of acid and base added, respectively; ΔQ_{blank} (mol/L) represents consumption or release of H^+ by side reactions; ΔQ_{solid} (mol/L) and ΔQ^H (mol/g) represent the proton excess of the Na-bentonite in different units, respectively; V (L) is the volume of aqueous solution and m (g) is the mass of the Na-bentonite.

Fig. 3 illustrates the titration results of the Na-bentonite at three ionic strengths (0.01, 0.1 and 0.5 mol/L NaCl). As seen in Fig. 3, the titration curves at three ionic strengths are parallel to each other. The degree of protonation increases with decreasing ionic strength. As a result, the point of zero charge (PZC) also increases with decreasing ionic strength. This is agreement with previous results of potentiometric titration for Na-montmorillonite [15,16,25].

It has ever been a challenge to account for the parallel titration curves of clay minerals by surface complexation model, because they are different from those for oxides. The characteristic feature of the acid-base titration results for oxides is that the titration curves have a common intersection point at PZC. In addition, the

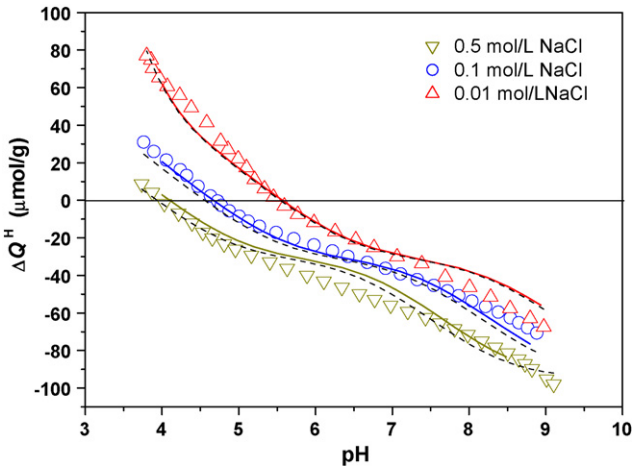

Fig. 3. Proton excess of the purified Na-bentonite as a function of pH at three ionic strengths. The points represent the experimental data. The dash lines illustrate the fitted results by FITEQL. The solid lines are the calculated results by PHREEQC.

degree of protonation of oxides at low pH usually increases with increasing ionic strength. In 1998, Kraepiel et al. [26] developed two surface complexation models to interpret the parallel titration curves of clay minerals. In model 1, the clay mineral is treated as nonpenetrable solid. Two kinds of surface sites are considered: X^- groups bearing a pH-independent charge and ≡SOH groups developing pH-dependent charge from protonation and deprotonation. The surface charge density of the solid is the sum of the permanent charge and pH-dependent charge. The relationship between surface charge and the surface potential is derived from Gouy-Chapman theory. In model 2, the clay mineral is treated as porous solid. The pH-independent groups are considered to be homogeneously located interior of the solid, while the ≡SOH groups are located on the surface of the solid at the interface with the aqueous solution. The relationship between potential and charge is calculated by Poisson–Boltzmann equation. The major difference of these two models is the calculation of potential from permanent negative charge [27]. In the present paper, a model similar with model 1 will be used.

Montmorillonite is 2:1 type phyllosilicate with layers composed of two silicon tetrahedral sheets sandwiching an aluminum octahedral sheet. Thus except for the layer site (permanently negatively charged site), X^-, two kinds of edge sites, aluminol and silanol, should be considered. In the present paper, ≡SOH is used to represent aluminol on octahedral sheets, while ≡YOH is used to represent silanol on tetrahedral sheets. The site density ratio of ≡YOH to that of ≡SOH was fixed to be 2 to minimize the number of adjustable parameters. Both protonation and deprotonation reactions on ≡SOH were assumed, while only deprotonation reaction on the site ≡YOH was considered [15]. In Na-form, the layer site of Na-bentonite, X^-, was assumed to be completely occupied by Na^+. The capacity of X^- site was fixed to be the measured CEC value. When the Na-bentonite was dispersed in aqueous solution, dissociation of XNa and combination of X^- and H^+ were considered. Thus, five reactions were used to account for the acid-base chemistry of the purified Na-bentonite:

$$X^- + Na^+ \rightleftharpoons XNa \quad (5)$$

$$X^- + H^+ \rightleftharpoons XH \quad (6)$$

$$\equiv SOH + H^+ \rightleftharpoons \equiv SOH_2^+ \quad (7)$$

$$\equiv SOH \rightleftharpoons \equiv SO^- + H^+ \quad (8)$$

$$\equiv YOH \rightleftharpoons \equiv YO^- + H^+ \quad (9)$$

According to reactions (5)–(9), the surface proton excess ΔQ^H (mol/g) can be expressed as:

$$\Delta Q^H = \frac{V}{m}([\equiv SOH_2^+] + [XH] - [\equiv SO^-] - [\equiv YO^-]) \quad (10)$$

The surface charge of the Na-bentonite ΔQ^{charge} (mol/g) can be calculated as:

$$\Delta Q^{charge} = \frac{V}{m}([\equiv SOH_2^+] - [\equiv SO^-] - [\equiv YO^-] - [X^-]) \quad (11)$$

The surface charge density σ (C/m^2) is given by:

$$\sigma = \frac{F}{s}\Delta Q^{charge} \quad (12)$$

where F is the Faraday constant (96485 C/mol); s (m^2/g) is the specific surface area of the Na-bentonite. The surface potential (Ψ, V) can be calculated by [8]:

$$\sigma = (8RT\varepsilon\varepsilon_0 c_e \times 10^3)^{1/2} \sinh\left(\frac{Z_e \psi F}{2RT}\right) \quad (13)$$

where ε is the dielectric constant of water (dimensionless, 78.5 at 25 °C), ε_0 the vacuum permittivity (8.854×10^{-12} C/V m), c_e the concentration of the background electrolyte, Z_e the valence of the symmetrical background electrolyte.

Table 3
Modeling parameters for potentiometric titration and Eu(III) surface complexation on the purified Na-bentonite.

Description of the purified Na-bentonite			
Specific surface area		53.6 m^2/g	
Sites		Site density	
X^-		1.16×10^{-5} mol/m^2 (623 meq/kg)	
≡SOH	≡S^{S}OH	1.88×10^{-8} mol/m^2	5.88×10^{-7} mol/m^2
	≡S^{W}OH	5.69×10^{-7} mol/m^2	
≡YOH		1.18×10^{-6} mol/m^2	

Aqueous solution/solid equilibria: reactions involved in acid-base titration	
Reactions	log K^{int}
$XNa \rightleftharpoons X^- + Na^+$	−1.3
$XNa + H^+ \rightleftharpoons XH + Na^+$	0.79
$\equiv S^SOH + H^+ \rightleftharpoons \equiv S^SOH_2^+$	3.23
$\equiv S^SOH \rightleftharpoons \equiv S^SO^- + H^+$	−3.89
$\equiv S^WOH + H^+ \rightleftharpoons \equiv S^WOH_2^+$	3.23
$\equiv S^WOH \rightleftharpoons \equiv S^WO^- + H^+$	−3.89
$\equiv YOH \rightleftharpoons \equiv YO^- + H^+$	−6.57

Aqueous solution/solid equilibria: surface complexation reactions of Eu(III)	
Reactions	log K^{int}
$3XNa + Eu^{3+} \rightleftharpoons X_3Eu + 3Na^+$	1.3
$\equiv S^SOH + Eu^{3+} \rightleftharpoons \equiv S^SOEu^{2+} + H^+$	1.3
$\equiv S^WOH + Eu^{3+} \rightleftharpoons \equiv S^WOEu^{2+} + H^+$	−2
$\equiv S^WOH + Eu^{3+} + H_2O \rightleftharpoons \equiv S^WOEuOH^+ + 2H^+$	−6.8
$\equiv S^WOH + Eu^{3+} + 3H_2O \rightleftharpoons \equiv S^WOEu(OH)_3^- + 4H^+$	−20.6
$\equiv S^WOH + Eu^{3+} + CO_3^{2-} \rightleftharpoons \equiv S^WOEuCO_3 + H^+$	8.2

The corresponding intrinsic constants of reactions (5)–(9) are respectively as follows:

$$K_1^{int} = \frac{[XNa]}{[X^-][Na^+]\gamma_{Na^+}} \exp\left(\frac{F\Psi}{RT}\right) \quad (14)$$

$$K_2^{int} = \frac{[XH]}{[X^-][H^+]\gamma_{H^+}} \exp\left(\frac{F\Psi}{RT}\right) \quad (15)$$

$$K_3^{int} = \frac{[\equiv SOH_2^+]}{[\equiv SOH][H^+]\gamma_{H^+}} \exp\left(\frac{F\Psi}{RT}\right) \quad (16)$$

$$K_4^{int} = \frac{[\equiv SO^-][H^+]\gamma_{H^+}}{[\equiv SOH]} \exp\left(\frac{-F\Psi}{RT}\right) \quad (17)$$

$$K_5^{int} = \frac{[\equiv YO^-][H^+]\gamma_{H^+}}{[\equiv YOH]} \exp\left(\frac{-F\Psi}{RT}\right) \quad (18)$$

The fitted parameters by the code FITEQL are listed in Table 3. As seen in Fig. 3, the titration curves are reasonably reproduced by the proposed model. It should be pointed out that the surface charge of the Na-bentonite (Eq. (11)) is different from the proton excess (Eq. (10)) because of reactions (5) and (6). The contribution of the permanent negative charge to the total surface charge of the Na-bentonite is the base to successfully interpret the parallel titration curves by surface complexation model. Moreover, it should be noted that the influence of the Na-bentonite dissolution could be neglected in the present case, because the maximum Al(III) concentration in the aqueous phase during titration was found to be only 2.5×10^{-5} mol/L and has very limited influence on the final titration results.

The parameters obtained by FITEQL were incorporated into the code PHREEQC and calculations were carried out for comparison. As seen in Fig. 3, PHREEQC gives almost identical results as those by FITEQL.

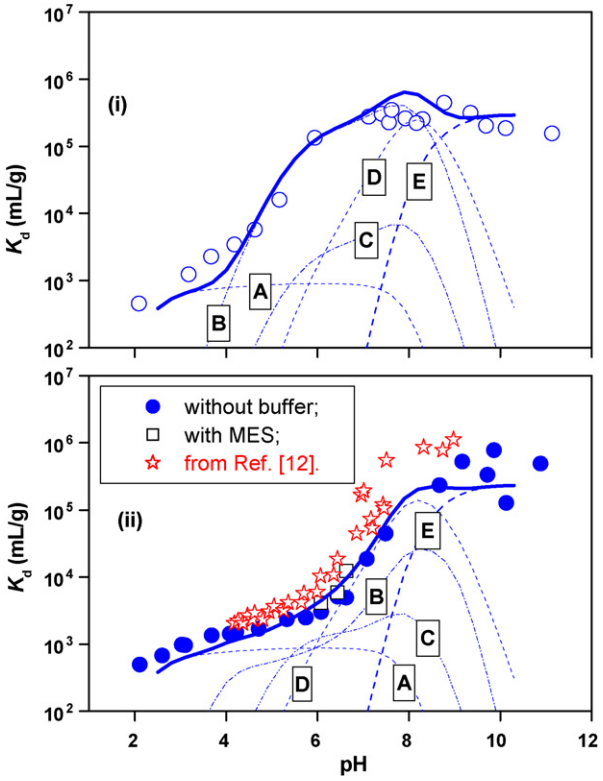

Fig. 4. pH adsorption edges of Eu(III) on the purified Na-bentonite in the absence of CO_2 at [NaCl] = 0.1 mol/L and m/V = 0.5 g/L; (i) $[Eu(III)]_{tot} = 6.74 \times 10^{-8}$ mol/L; (ii) $[Eu(III)]_{tot} = 3.33 \times 10^{-6}$ mol/L. The points represent the experimental data. The solid lines are calculated by the proposed model. The dash lines illustrate the contributions of different surface species to Eu(III) adsorption: (A) X_3Eu; (B) $\equiv S^SOEu^{2+}$; (C) $\equiv S^WOEu^{2+}$; (D) $\equiv S^WOEuOH^+$; (E) $\equiv S^WOEu(OH)_3^-$.

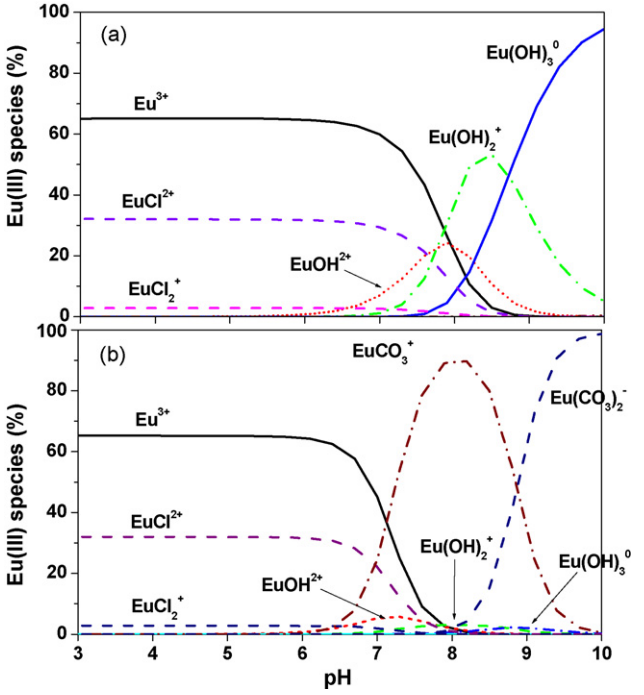

Fig. 5. Eu(III) speciation in 0.1 mol/L NaCl solution; (a) in the absence of CO_2; (b) in equilibrium with CO_2 at $P_{CO_2} = 10^{-3.58}$ atm; $[Eu(III)]_{tot} = 3.33 \times 10^{-6}$ mol/L.

3.2. pH adsorption edges of Eu(III) in the absence of CO_2

pH adsorption edges of Eu(III) in the absence of CO_2 at $[Eu(III)]_{tot} = 3.33 \times 10^{-6}$ and 6.74×10^{-8} mol/L are shown in Fig. 4. The adsorption edges present three distinct parts: (i) Below pH 4, the adsorption of Eu(III) increases slightly with pH; (ii) In the pH range of 4–8, the slopes of the Eu(III) adsorption edges increase significantly with pH in comparison with the previous pH range; (iii) Above pH 8, the adsorption of Eu(III) reaches about 95% and keeps almost constant with pH. Similar profiles of pH adsorption edges were found for U(VI) adsorption on Na-montmorillonite [28]. For comparison, a pH adsorption edge of Eu(III) on SWy-1 Na-montmorillonite reported by Bradbury and Baeyens [12] under similar conditions ($[Eu(III)]_{tot} = 1.3 \times 10^{-7}$ mol/L, $[NaClO_4] = 0.1$ mol/L, m/V = 1.5 g/L) was also presented in Fig. 4(ii). Two results are comparable although the sorbents are different from origins, chemical compositions and even the acid-base chemistry [9].

As seen in Fig. 5(a), Eu^{3+} is the dominant species in aqueous solution up to pH 7.5. Thus the first sorbate considered in modeling should be free Eu^{3+}. The reaction between XNa and Eu^{3+} can be written as:

$$3XNa + Eu^{3+} \rightleftharpoons X_3Eu + 3Na^+ \quad (19)$$

$$K_6 = \frac{[XNa]^3[Eu^{3+}]}{[X_3Eu][Na^+]^3}\frac{\gamma_{Eu^{3+}}}{\gamma_{Na^+}^3} \quad (20)$$

As seen in Fig. 4, it is obvious that only reaction (19) cannot interpret the rising pH adsorption edges. The equilibrium constant of reaction (19) was adjusted to get good fits for the adsorption data at pH ≤ 4. Surface complexation reactions on edge sites must be considered. Tertre et al. [15] has pointed out that the surface complexes on edge sites of montmorillonite are mainly bound on the site of aluminol based on a research of Time Resolved Laser Fluorescence Spectroscopy (TRLFS). Therefore, only surface complexation reactions of Eu(III) on ≡SOH were considered in this paper. The surface complexation reaction of Eu^{3+} on ≡SOH and the corresponding intrinsic equilibrium constant can be respectively expressed as:

$$\equiv SOH + Eu^{3+} \rightleftharpoons \equiv SOEu^{2+} + H^+ \quad (21)$$

$$K_7^{int} = \frac{[\equiv SOEu^{2+}][H^+]}{[\equiv SOH][Eu^{3+}]}\frac{\gamma_{H^+}}{\gamma_{Eu^{3+}}}\exp\left(\frac{2F\Psi}{RT}\right) \quad (22)$$

At pH > 7.5, Eu(III) hydrolysis products, such as $EuOH^{2+}$, $Eu(OH)_2^+$ and $Eu(OH)_3^0$, successively become dominant Eu(III) species in aqueous phase (Fig. 5(a)). All these species are potential sorbates in the high pH range and should be considered in modeling calculations.

$$\equiv SOH + Eu^{3+} + H_2O \rightleftharpoons \equiv SOEuOH^+ + 2H^+ \quad (23)$$

$$\equiv SOH + Eu^{3+} + 2H_2O \rightleftharpoons \equiv SOEu(OH)_2 + 3H^+ \quad (24)$$

$$\equiv SOH + Eu^{3+} + 3H_2O \rightleftharpoons \equiv SOEu(OH)_3^- + 4H^+ \quad (25)$$

The corresponding intrinsic constants for reactions (23)–(25) are as follows:

$$K_8^{int} = \frac{[\equiv SOEuOH^+][H^+]^2}{[\equiv SOH][Eu^{3+}]}\frac{\gamma_{H^+}^2}{\gamma_{Eu^{3+}}}\exp\left(\frac{F\Psi}{RT}\right) \quad (26)$$

$$K_9 = \frac{[\equiv SOEu(OH)_2][H^+]^3}{[\equiv SOH][Eu^{3+}]}\frac{\gamma_{H^+}^3}{\gamma_{Eu^{3+}}} \quad (27)$$

$$K_{10}^{int} = \frac{[\equiv SOEu(OH)_3^-][H^+]^4}{[\equiv SOH][Eu^{3+}]}\frac{\gamma_{H^+}^4}{\gamma_{Eu^{3+}}}\exp\left(\frac{-F\Psi}{RT}\right) \quad (28)$$

From modeling exercise, it was found that it is impossible to simultaneously fit the pH adsorption edges at two different Eu(III) concentrations (Fig. 4) with the above surface reactions.

The pH adsorption edge at $[Eu(III)]_{tot} = 6.74 \times 10^{-8}$ mol/L would be underestimated when a proper fit was obtained for that at $[Eu(III)]_{tot} = 3.33 \times 10^{-6}$ mol/L. On the contrary, if the adsorption edge at $[Eu(III)]_{tot} = 6.74 \times 10^{-8}$ mol/L was well reproduced, the adsorption edge at $[Eu(III)]_{tot} = 3.33 \times 10^{-6}$ mol/L would be overestimated.

Surface sites with same hydrolysis constants but different affinities for a metal cation have been proposed in many studies [9–14,27]. This should be a good strategy to solve the above problem. Two sub sites with same hydrolysis constants as those for ≡SOH but different affinities for Eu(III) were proposed in this study (see Table 3). $\equiv S^SOH$ and $\equiv S^WOH$ were used to represent the strong and weak bonding sites for Eu(III), respectively. The sum of two sites densities is equal to that of ≡SOH obtained by fitting the titration results. From modeling exercise, an estimation of site densities of $\equiv S^SOH$ and $\equiv S^WOH$ was obtained when the pH adsorption edges where reaction (21) on the sites $\equiv S^SOH$ and $\equiv S^WOH$ works were well fitted. Then reactions (23)–(25) on the sites $\equiv S^SOH$ and $\equiv S^WOH$ were successively considered. It was found that not all of reactions (23)–(25) on the sites $\equiv S^SOH$ and $\equiv S^WOH$ were needed to get a reasonable fit for the Eu(III) pH adsorption edges. Besides reaction (21) on $\equiv S^SOH$ and $\equiv S^WOH$ and reaction (19), reactions (23) and (25) on $\equiv S^WOH$ were needed to reproduce the Eu(III) pH adsorption edges. Other reactions, such as (23)–(25) on $\equiv S^SOH$ and (24) on $\equiv S^WOH$ were found to be unimportant. The surface complexation reactions and the corresponding equilibrium constants used in modeling calculations are listed in Table 3.

Adsorption of cations on montmorillonite has also been interpreted in terms of cation exchange and surface complexation [9–15]. Gaines and Tomas convention of cation exchange has been used to account for cation adsorption on layer site [9–15]. According to this theory, the distribution coefficient of Eu(III) should be constant and independent of pH when cation exchange is the dominant adsorption mechanism in the low pH range [12]. However, as seen in Figs. 4 and 6, the adsorption of Eu(III) slightly decreases with decreasing pH at pH < 4. Similar results were also observed for U(VI) adsorption on Na-montmorillonite [28]. The decrease of adsorption with decreasing pH can be well explained by competition between metal ions and H^+ on the layer site. In the present case, the decrease of Eu(III) adsorption with decreasing pH at pH < 4 results from reactions (5), (6) and (19).

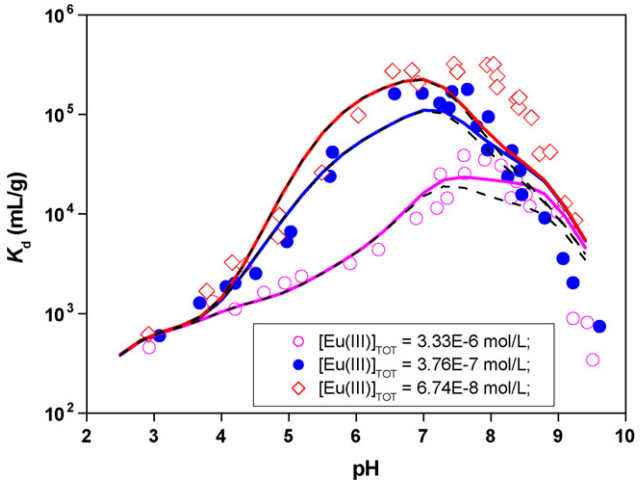

Fig. 6. pH adsorption edges of Eu(III) on the purified Na-bentonite in the presence of CO_2 at $P_{CO_2} = 10^{-3.58}$atm, $m/V = 0.5$ g/L, [NaCl] = 0.1 mol/L and different Eu(III) concentrations. The points show the experimental data. The dash lines are calculated by the model without $\equiv S^WOEuCO_3$. The solid lines are calculated by the model with the ternary surface complex $\equiv S^WOEuCO_3$.

3.3. pH adsorption edges of Eu(III) in the presence of CO_2 at $P_{CO_2} = 10^{-3.58}$ atm

Three pH adsorption edges of Eu(III) on the Na-bentonite in the presence of CO_2 ($P_{CO_2} = 10^{-3.58}$atm) were collected to evaluate the influence of CO_2. As shown in Fig. 6, the adsorption of Eu(III) decreases with pH at pH > 8. The decrease of Eu(III) adsorption with pH can be interpreted by the complexation of Eu(III) and carbonate in aqueous phase. Furthermore, it was found that the presence of CO_2 has little influence on Eu(III) adsorption at pH < 7 in comparison with that in the absence of CO_2.

As shown in Fig. 5(b), the hydrolysis products of Eu(III) in aqueous solution are suppressed in the presence of CO_2 ($P_{CO_2} = 10^{-3.58}$atm). The aqueous Eu(III) complexes of carbonate such as $EuCO_3^+$ and $Eu(CO_3)_2^-$ are the dominant Eu(III) species in the high pH range. Therefore, it should be evaluated whether ternary surface complexes of Eu(III) and carbonate were formed. Modeling exercise can help to answer this question. The calculated results by the above model without considering any ternary surface complexes of carbonate are shown in Fig. 6 as dash lines. It is obvious that the adsorption of Eu(III) around pH 8 is somewhat underestimated in this case. Thus ternary surface complexes of carbonate should be considered. Because $EuCO_3^+$ is the dominant Eu(III) species in aqueous solution at pH ~8 (Fig. 5(b)), the first ternary surface complexation reaction can be expressed as:

$$\equiv SOH + Eu^{3+} + CO_3^{2-} \rightleftharpoons \equiv SOEuCO_3 + H^+ \quad (29)$$

$$K_{11} = \frac{[\equiv SOEuCO_3][H^+]}{[\equiv SOH][Eu^{3+}][CO_3^{2-}]} \frac{\gamma_{H^+}}{\gamma_{Eu^{3+}}\gamma_{CO_3^{2-}}} \quad (30)$$

In modeling practice, only reaction (29) on $\equiv S^WOH$ was considered because of its relatively high site density. As seen in Fig. 6, reaction (29) improves the fitting goodness to some extent. However, the pH adsorption edge at $[Eu(III)]_{tot} = 6.74 \times 10^{-8}$ mol/L is still underestimated at pH ~8. Further modeling exercises demonstrated that other ternary surface complexes of carbonate cannot improve the fitting goodness.

3.4. Adsorption and desorption isotherms of Eu(III)

Eu(III) adsorption and desorption isotherms at pHs 4, 6, 6.5 and 7.5 in the absence of CO_2 are shown in Fig. 7(i)–(iv), respectively. The adsorption and desorption isotherms at a given pH are almost on the same line, which demonstrates that the Eu(III) adsorption/desorption on the Na-bentonite are reversible. This is the base for modeling Eu(III) adsorption in the framework of equilibration. Moreover, it was found that the buffers, MES and MOPS (2×10^{-3} mol/L), have little influence on Eu(III) adsorption (Fig. 7 (iii)–(iv)) and that the K_d values are independent of m/V (Fig. 7(iii)).

As seen in Fig. 7, the adsorption/desorption isotherms are reasonably reproduced by the proposed model, except that the adsorption/desorption isotherms at pH 7.5 is somewhat underestimated at $[Eu(III)] > 1 \times 10^{-6}$ mol/L. The contributions of different surface species to the overall adsorption are also illustrated in Fig. 7(i)–(iv). It should be noted that surface complexation reaction of Eu^{3+} on the site $\equiv S^SOH$ plays a same important role as cation exchange reaction (19) at pH 4 and $[Eu(III)] < 1 \times 10^{-6}$ mol/L (Fig. 7(i)). Moreover, it is obvious that reaction (19) is the main adsorption mechanism at $[Eu(III)] > 6 \times 10^{-5}$ mol/L (Fig. 7(i)–(iv)).

For comparison, an adsorption isotherm of Eu(III) on Na-montmorillonite at pH 6, $[NaClO_4] = 0.1$ mol/L and $m/V = 0.5$ g/L reported by Bradbury and Baeyens [12] is also presented in Fig. 7(ii). Two adsorption isotherms at $[Eu(III)] < 10^{-5}$ mol/L are identical, whereas the K_d values for SWy-1 Na-montmorillonite [12] at $[Eu(III)] > 10^{-5}$ mol/L are somewhat higher than those in the present

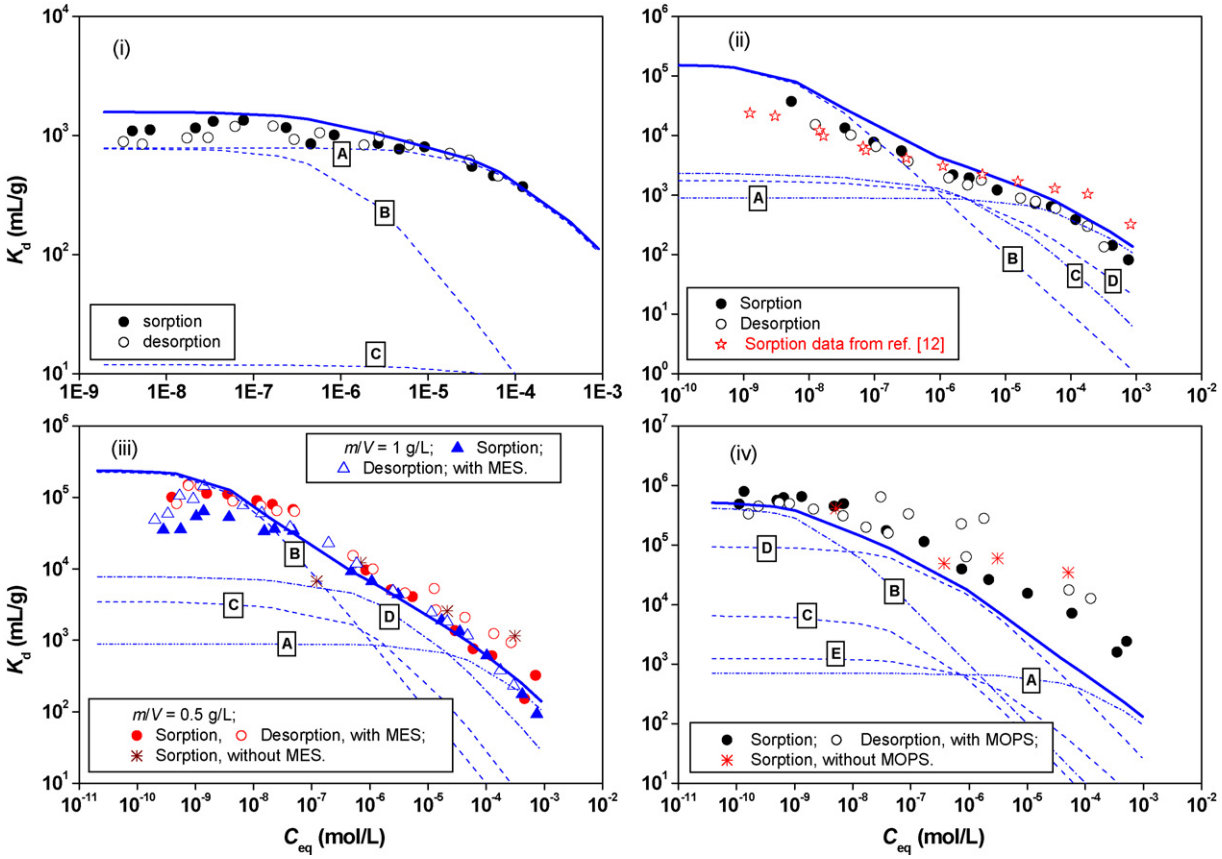

Fig. 7. Adsorption and desorption isotherms of Eu(III) on the purified Na-bentonite in the absence of CO_2 at [NaCl] = 0.1 mol/L; (i) pH 4.04 ± 0.05 and m/V = 1 g/L; (ii) pH 6.01 ± 0.05 and m/V = 1 g/L; (iii) pH 6.53 ± 0.05; (iv) pH 7.46 ± 0.10 and m/V = 0.25 g/L. The points show the experimental data. The solid lines represent the results calculated by the proposed model. The dash lines illustrate the contributions of different surface complexes to Eu(III) adsorption: (A) X_3Eu; (B) $\equiv S^SOEu^{2+}$; (C) $\equiv S^WOEu^{2+}$; (D) $\equiv S^WOEuOH^+$; (E) $vS^WOEu(OH)_3^-$.

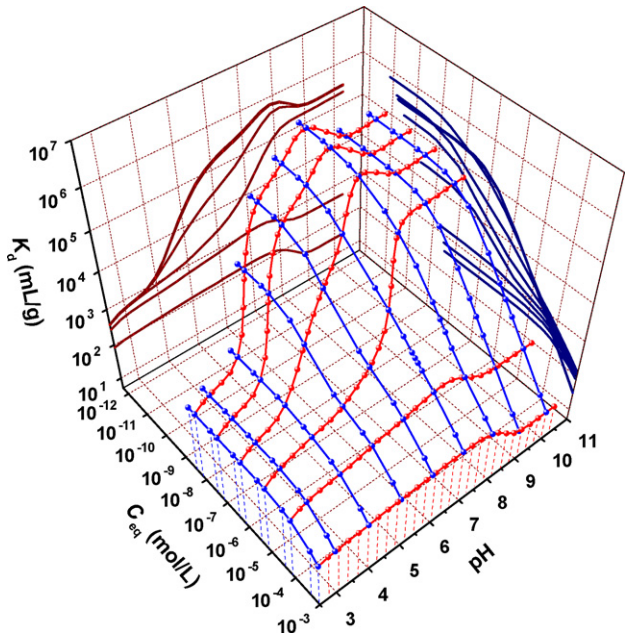

Fig. 8. The dependence of Eu(III) distribution coefficient (K_d) on Eu(III) concentration (C_{eq}) and pH in the absence of CO_2 at [NaCl] = 0.1 mol/L and m/V = 1 g/L.

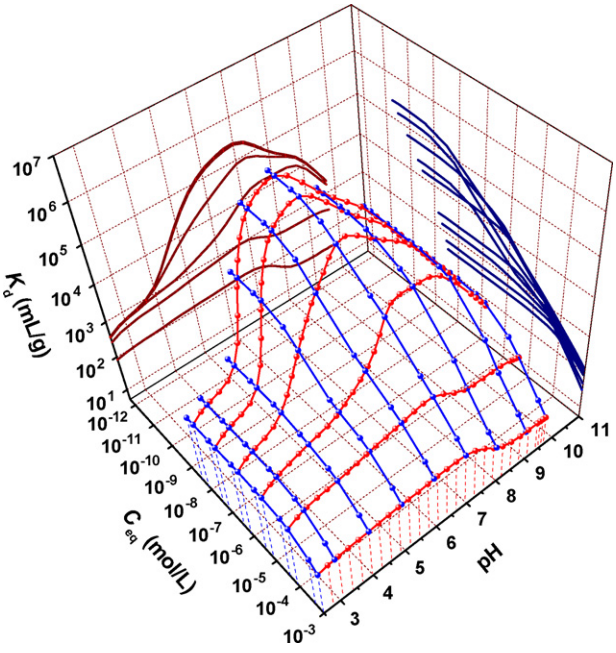

Fig. 9. The dependence of Eu(III) distribution coefficient (K_d) on Eu(III) concentration (C_{eq}) and pH in the presence of CO_2 at $P_{CO_2} = 10^{-3.58}$ atm, [NaCl] = 0.1 mol/L and m/V = 1 g/L.

study. Considering that cation exchange reaction between XNa and Eu^{3+} is the main mechanism at high Eu(III) concentrations, the difference may be resulted from different CEC values of the two sorbents.

3.5. The relationships between K_d, C_{eq}, and pH

The relationships between K_d, C_{eq} and pH in the absence and presence of CO_2 given by the model are illustrated as three dimensional plots in Figs. 8 and 9, respectively. The projections on the K_d-pH plane represent the pH adsorption edges at different Eu(III) concentrations, while those on the K_d–C_{eq} plane illustrate the adsorption isotherms at variable pHs. As seen in Figs. 8 and 9, plateaus of K_d values in the absence and presence of CO_2 would occur at pH ~8. This information would be valuable in nuclear waste management, because the pH values of raw bentonite suspensions are usually controlled by the clay itself to be ~8.

4. Conclusions

The acid–base chemistry of a purified Na-bentonite was evaluated by continuous potentiometric titrations at 25 °C. The titration curves at three ionic strengths (0.01, 0.1 and 0.5 mol/L NaCl) are parallel and have no common intersection point. The point of zero charge (PZC) of the purified Na-bentonite increases with deceasing ionic strength. The experimental titration curves were successfully interpreted by a double layer model, which involves three sites, i.e., one layer site and two edge sites. The adsorption/desorption of Eu(III) on the Na-bentonite were studied under wide experimental conditions at 22 ± 2 °C. The reversibility of the Eu(III) adsorption/desorption on the Na-bentonite was demonstrated by adsorption/desorption isotherms. pH adsorption edges of Eu(III) in the absence and presence of CO_2 ($P_{CO_2} = 10^{-3.58}$ atm) were reasonably interpreted by a surface complexation model. The adsorption isotherms were reproduced by the model. The model predicts that the plateau of K_d values would occur at pH ~8, when the partial pressure of CO_2 is between 0–$10^{-3.58}$ atm.

Acknowledgment

The financial support by the National Natural Science Foundation of China (Nos. 20501010 and J0630962) is gratefully appreciated.

References

[1] J. Wilson, D. Savage, J. Cuadros, M. Shibata, K.V. Ragnarsdottir, The effect of iron on montmorillonite stability. (I) Background and thermodynamic considerations, Geochim. Cosmochim. Acta 70 (2006) 306–322.
[2] T. Shahwan, H.N. Erten, S. Unugur, A characterization study of some aspects of the adsorption of aqueous Co^{2+} ions on a natural bentonite clay, J. Colloid Interface Sci. 300 (2006) 447–452.
[3] A. Bauer, T. Rabung, F. Claret, T. Schafer, G. Buckau, T. Fanghanel, Influence of temperature on sorption of europium onto smectite: The role of organic contaminants, Applied Clay Sci. 30 (2005) 1–10.
[4] Th. Rabung, M.C. Pierret, A. Bauer, H. Geckeis, M.H. Bradbury, B. Baeyens, Sorption of Eu(III)/Cm(III) on Ca-montmorillonite and Na-illite. Part 1: Batch sorption and time-resolved laser fluorescence spectroscopy experiments, Geochim. Cosmochim. Acta 69 (2005) 5393–5402.
[5] E. Tertre, G. Berger, S. Caster, M. Loubet, E. Giffaut, Experimental sorption of Ni^{2+}, Cs^{+} and Ln^{3+} onto a montmorillonite up to 150 °C, Geochim. Cosmochim. Acta 69 (2005) 4937–4948.
[6] J.G. Catalano, G.E.J.R. Brown, Uranyl adsorption onto montmorillonite: evaluation of binding sites and carbonate complexation, Geochim. Cosmochim. Acta 69 (2005) 2995–3005.
[7] J. Ikhsan, J.D. Wells, B.B. Johnson, M.J. Angove, Surface complexation modeling of the sorption of Zn(II) by montmorillonite, Colloids Surf. A: Physicochem. Eng. Aspects 252 (2005) 33.
[8] D.A. Dzombak, F.M.M. Morel, Surface Complexation Modeling: Hydrous Ferric Oxide, Wiley-Interscience, New York, 1990.
[9] B. Baeyens, M.H. Bradbury, A mechanistic description of Ni and Zn sorption on Na-montmorillonite Part I: titration and sorption measurements, J. Contam. Hydrol. 27 (1997) 199–222.
[10] M.H. Bradbury, B. Baeyens, A mechanistic description of Ni and Zn sorption on Na-montmorillonite Part II: modeling, J. Contam. Hydrol. 27 (1997) 223–248.
[11] M.H. Bradbury, B. Baeyens, Modelling the sorption of Zn and Ni on Ca-montmorillonite, Geochim. Cosmochim. Acta 63 (1999) 325–336.
[12] M.H. Bradbury, B. Baeyens, Sorption of Eu on Na- and Ca-montmorillonites: experimental investigations and modelling with cation exchange and surface complexation, Geochim. Cosmochim. Acta 66 (2002) 2325–2334.
[13] M.H. Bradbury, B. Baeyens, Experimental measurements and modeling of sorption competition on montmorillonite, Geochim. Cosmochim. Acta 69 (2005) 4187–4197.
[14] M.H. Bradbury, B. Baeyens, H. Geckeis, Th. Rabung, Experimental measurements and modeling of sorption competition on montmorillonite, Geochim. Cosmochim. Acta 69 (2005) 5403–5412.
[15] E. Tertre, G. Berger, E. Simoni, S. Castet, E. Giffaut, M. Loubet, H. Catalette, Europium retention onto clay minerals from 25 to 150 °C: Experimental measurements, spectroscopic features and sorption modeling, Geochim. Cosmochim. Acta 70 (2006) 4563–4578.
[16] M. Duc, F. Gaboriaud, F. Thomas, Sensitivity of the acid–base properties of clays to the methods of preparation and measurement: 2. Evidence from continuous potentiometric titrations, J. Colloid Interface Sci. 289 (2005) 148–156.
[17] E. Tertre, S. Castet, G. Berger, M. Loubet, E. Giffaut, Geochim, Surface chemistry of kaolinite and Na-montmorillonite in aqueous electrolyte solutions at 25 and 60 °C: experimental and modeling study, Cosmochim. Acta 70 (2006) 4579–4599.
[18] C. Tournassat, J.M. Greneche, D. Tisserand, L. Charlet, The titration of clay minerals: I. Discontinuous backtitration technique combined with CEC measurements, J. Colloid Interface Sci. 273 (2004) 224–233.
[19] C. Poinssot, B. Baeyens, M.H. Bradbury, Experimental studies of Cs, Sr, Ni, and Eu sorption on Na-illite and the modeling of Cs sorption, PSI Bericht Nr. 99-06, August 1999, ISSN 1019-0643 P6.
[20] D.L. Sparks, Environmental Soil Chemistry, 2nd ed., Academic Press, Elsevier Science, USA, 2003, p. 70.
[21] M.H. Bradbury, B. Baeyens, Porewater chemistry in compacted re-saturated MX-80 bentonite: physic-chemical characterization and geochemical modeling, PSI Bericht Nr. 02-10, June 2002, ISSN 1019-0643 P31.
[22] A. Herbelin, J. Westall, FITEQL A Computer Program for Determination of Chemical Equilibrium Constants From Experimental Data Version 3. 1, Department of Chemistry, Oregon State University, Oregon, 1994.
[23] D.L. Parkhurst, C.A.J. Appelo, User's guide to PHREEQC (Version 2)—a computer program for speciation, batch-reaction, one-dimensional transport, and inverse geochemical calculations, U.S.G.S. Water-Resources Report 99-4259, 1999.
[24] W. Hummel, U. Berner, E. Curti, F.J. Pearson, T. Thoenen, Nagra/PSI Chemical Thermodynamic Data Base 01/01. Universal Publishers/uPUBLISH.com USA, available from: http://www.upublish.com/books/hummel.htm. Also issued as Nagra Technical Report NTB 02-16, Nagra, Wettingen, Switzerland, 2002.
[25] H. Wanner, Y. Albinsson, O. Karnland, E. Wieland, P. Wersin, L. Charlet, The acid/base chemistry of montmorillonite, Radiochim. Acta 66/67 (1994) 157–162.
[26] A.M.L. Kraepiel, K. Keller, F.M.M. Morel, On the acid–base chemistry of permanently charged minerals, Environ. Sci. Technol. 32 (1998) 2829–2838.
[27] M. Hoch, R. Weerasooriya, New model calculations of pH-depending tributyltin adsorption onto montmorillonite surface and montmorillonite-rich sediment, Environ. Sci. Technol. 39 (2005) 844–849.
[28] A. Kowal-Fouchard, R. Drot, E. Simoni, J.J. Ehrhardt, Use of spectroscopic techniques for uranium(VI)/montmorillonite interaction modeling, Environ. Sci. Technol. 38 (2004) 1399–1407.